AIAA Aviation Forum and ASCEND co-located Conference Proceedings
29 July - 2 August 2024, Las Vegas, Nevada
AIAA AVIATION FORUM AND ASCEND 2024
10.2514/6.2024-3589

Flapped CoFlow Jet Wing for High Lift Cruise in the Martian Atmosphere

Jaehyoung Jeon * Yan Ren † Gecheng Zha ‡
Dept. of Mechanical and Aerospace Engineering
University of Miami, Coral Gables, Florida 33124
E-mail: gzha@miami.edu

Abstract

This paper studies the potential of a flapped coflow jet (FCFJ) wing design to achieve ultra-high cruise lift coefficients (C_L) under low Reynolds number conditions in the Martian atmosphere. Building upon prior research demonstrating high cruise C_L on a 2D FCFJ airfoil, this study investigates the performance of 3D wings constructed using the same airfoil, with a focus on understanding the impact of induced drag on overall aerodynamic efficiency. Computational fluid dynamics (CFD) simulations were conducted using a validated 3D RANS solver incorporating the Spalart-Allmaras (SA) turbulence model, a third-order WENO scheme for inviscid fluxes, and second-order central differencing for viscous terms. The investigation centered on a 3D FCFJ wing with an aspect ratio (AR) of 20 at a Mach number (M) of 0.17 and a Reynolds number R_e of 5.63×10^4. A extraordinarily high cruise C_L of 3.5 and a corrected lift-to-drag ratio $(C_L/C_D)_c$ of 7.5 are obtained using a circular tip cap, a flap deflection angle β of 35°, and an injection size of 0.6%C. These results in an ultra-high productivity efficiency $(C_L^2/C_D)_c$ of 26.25 at a very low Reynolds number. This research has laid an important foundation for the design of a fixed wing aircraft capable of ultra-high cruise C_L and productivity efficiency to fly in thin Martian atmosphere.

Nomenclature

CFJ	CoFlow jet
$FCFJ$	Flapped CoFlow jet
$AoA(\alpha)$	Angle of attack
β	Deflection angle
LE	Leading Edge
TE	Trailing Edge
s	Wing Span length
c	Profile chord
U	Flow velocity

* Ph.D. Student
† Postdoc Researcher, Ph.D., AIAA member
‡ Professor, ASME Fellow, AIAA associate Fellow

q	Dynamic pressure $0.5\,\rho\,U^2$
p	Static pressure
T	Static temperatue
ρ	Air density
μ	Dynamic viscosity
R	Specific gas constant
P	Pumping power
C_L	Lift coefficient $L/(q_\infty\,S)$
C_D	Drag coefficient $D/(q_\infty\,S)$
C_μ	Jet momentum coef. $\dot{m}_j\,U_j/(q_\infty\,S)$
Pc	Power coefficient $P/(q_\infty\,S\,V_\infty)$
$(C_L/C_D)_c$	CFJ airfoil corrected efficiency $C_L/(C_D$+Pc)
R_e	Reynolds number
M	Mach number
c_p	Constant pressure specific heat
γ	Air specific heats ratio
S	Planform area of the wing
T_t	Total temperature
P_t	Total pressure
H_t	Total specific enthalpy
$\dot{m}$	Mass flow across the pump
$_\infty$	Subscript, stands for free stream
$_j$	Subscript, stands for jet

1 Introduction

The growing interest and research in Mars exploration necessitates technological advancements to increase the mobility range on Martian surface by aerial robots. However, the Martian environment presents unique challenges for air transportation due to its thin atmosphere and diverse terrain. To address these challenges, high-performance, high-efficiency aircraft specifically designed for Mars are crucial for future exploration. These aircraft offer numerous benefits, including enhanced mobility and accessibility for exploring vast Martian landscapes, facilitating resource discovery and identifying the existence of water, ice, methane, and study the Martial geology history. A key challenge in developing these aircraft lies in generating ultra-high lift coefficient to reduce the size and weight of the vehicle in the thin Martian atmosphere, characterized by low Reynolds numbers and low air density. Mars' significantly lower atmospheric density, about 100 times less than Earth's, necessitates innovative aircraft technologies. While Earth-based aircraft rely on air-wing interactions to generate lift, the thin Martian atmosphere poses a formidable challenge for achieving the necessary lift for sustained flight. This distinct atmospheric characteristic demands a paradigm shift in aerodynamic design to achieve optimal performance on Mars. Potential solutions include significantly larger wing area, aspect ratio, lower wing loading, and novel control surfaces specifically tailored to the Martian environment [1].

Active flow control (AFC) has emerged as a promising technology to improve aerodynamic performance at low Reynolds number, particularly for increasing maximum lift coefficient (C_{Lmax}) by suppressing flow separation and enhancing airfoil circulation. This is achieved by adding energy to the flow, typically

through techniques such as blowing or suction. However, applying AFC for cruise condition presents a significant challenge. While the benefits of increased C_{Lmax} are evident, they need to outweigh the energy consumption associated with the AFC to achieve a net system efficiency gain. One promising AFC technology with the potential to overcome this challenge and enhance cruise efficiency is the CoFlow Jet (CFJ) flow control airfoil[2, 3, 4, 5, 6, 7, 8, 9, 10, 11, 12, 13, 14, 15, 16, 17]. As shown in Fig. 1, the CFJ airfoil utilizes a series of micro-compressor actuators embedded within the airfoil. These actuators withdraw a small amount of the mass flow near trailing edge, pressurize it, and eject it tangent to the airfoil surface near leading edge, which energizes the boundary layer and keeps the flow attached under extreme adverse pressure gradients[18, 19]. In comparison with the 2D baseline airfoil, Wang and Zha[20] show that the 2D CFJ airfoil can achieve a significantly higher cruise lift coefficient and aerodynamic efficiency, defined as

$$(\frac{C_L}{C_D})_c = \frac{C_L}{C_D + P_c} \tag{1}$$

To achieve high cruise efficiency, it is necessary to have low CFJ power requirement, denoted by the CFJ required power coefficient, Pc. To assess the transportation productivity of aircraft, a parameter encompassing both range and gross weight is introduced: cruise productivity efficiency. This metric, proposed by Yang et al. [13], provides a more holistic evaluation of aircraft performance, considering not just aerodynamic efficiency but also payload capacity and range capability.

$$(\frac{C_L^2}{C_D})_c = \frac{C_L^2}{(C_D + Pc)} \tag{2}$$

CFJ wing can have substantially higher cruise C_L and thus greater productivity efficiency as well. Taking advantage of the CFJ wing high cruise lift coefficient and thus high suction effect on wing upper surface, Ren and Zha [21] design a tandem wing aircraft configuration that the front wing tip vortex is captured by the rear wing to enhance the overall system efficiency. However, for cruise condition, the regular CFJ configuration as shown in Fig. 1 appears to have rapid energy consumption increase when C_L is greater than 1.6[13, 22]. Even though the aerodynamic drag coefficient C_D can remain small and the pure aerodynamic lift to drag ratio C_L/C_D can be still very high, the corrected aerodynamic efficiency defined in Eq. (1) can decrease quickly with the increasing C_L.

The purpose of this paper is to devise a high lift coefficient and high productivity efficiency wing for low Reynolds number conditions on Mars. These features will bring essential feasibility to fly on Mars. The high productivity efficiency with high lift coefficient will allow a compact and light vehicle with a high payload. It will also allow the aircraft to fly at a lower speed to reduce propulsion power, which is proportional to the cube of flight velocity.

Flapped CoFlow Jet technology has emerged as a promising solution for achieving high C_L while maintaining a good $(C_L/C_D)_c$. This capability makes it particularly relevant for aircraft operating in low-density environments, such as at high altitudes on Earth or in the Martian atmosphere. As demonstrated in previous studies[23, 24], flapped CFJs can significantly enhance lift performance, opening opportunities for various flight applications. Notably, a 2D flapped CFJ study [25] achieved a remarkable $(C_L/C_D)_c$ of 20.5 while simultaneously maintaining a high C_L of 3.74 at a Mach number of 0.26 and a Reynolds number of 1.42×10^5. However, for low Reynolds number environment in Martian atmosphere, a Mach number of 0.17 and a Reynolds number of 5.63×10^4 are more desirable based on our trade studies to have high aerodynamic efficiency and low CFJ power required. Under these conditions, the 2D study

demonstrates a C_L exceeding 3.5 and a $(C_L/C_D)_c$ of approximately 16.2, highlighting the potential of flapped CFJ technology for significantly improved aerodynamic performance at low Reynolds conditions.

Building upon these promising findings, the present study is to numerically study the 3D flapped CFJ wing under low Reynolds number conditions of Martian atmosphere.

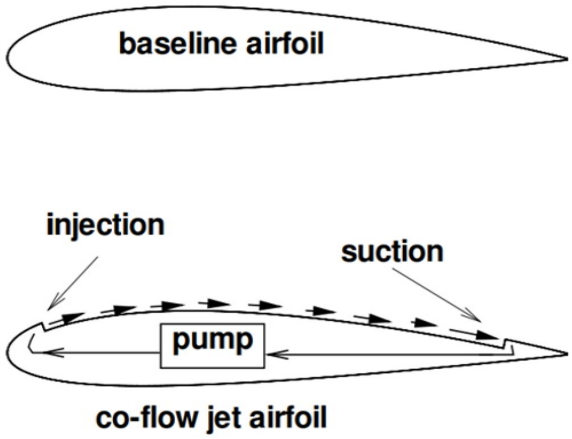

Figure 1: Sketch of CoFlow Jet airfoil

1.1 Flapped CoFlow Jet Airfoil

The concept of flapped coflow jet airfoil is adopted from the CFJ airfoil with deflected slipstream for VTOL aircraft [26]. It is also guided by the CoFlow jet flow separation mechanism study of Xu and Zha [27].

The CFJ is applied inside a long flap that is a part of the flapped CFJ airfoil, as shown in Fig.2 [23], which has the injection located at the shoulder of the flap. The regular CFJ airfoil applies the injection very close to the leading edge at a point of around 2-4% Chord location. By deflecting the flap rather than rotating the front of the airfoil, the FCFJ airfoil has the advantage of allowing the airfoil to change the angle of attack and lift coefficient without tilting the wings or the aircraft. The purpose of this paper is to demonstrate numerically that the FCFJ airfoil is a promising candidate to provide ultra-high cruise lift coefficient for 3D wing that can be used in low Reynolds number conditions of Martian atmosphere.

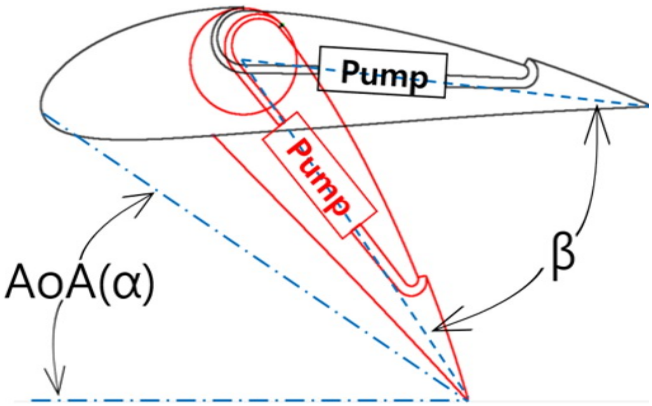

Figure 2: Sketch of flapped CFJ airfoil with the CoFlow jet applied on the flap

2 Methodology

2.1 Lift and Drag Calculation

The momentum and pressure at the injection and suction slots produce a reactionary force, which must included in CFD simulation. Using control volume analysis, the reactionary force can be calculated using the flow parameters at the injection and suction slot opening surfaces. Zha et al. [3] give the following formulations to calculate the lift and drag due to the jet reactionary force for a CFJ airfoil. By considering the effects of injection and suction jets on the CFJ airfoil, the expressions for these reactionary forces are given as :

$$F_{x_{cfj}} = (\dot{m}_j V_{j1} + p_{j1} A_{j1}) * cos(\theta_1 - \alpha) - (\dot{m}_j V_{j2} + p_{j2} A_{j2}) * cos(\theta_2 + \alpha) \tag{3}$$

$$F_{y_{cfj}} = (\dot{m}_{j1} V_{j1} + p_{j1} A_{j1}) * sin(\theta_1 - \alpha) + (\dot{m}_{j2} V_{j2} + p_{j2} A_{j2}) * sin(\theta_2 + \alpha) \tag{4}$$

where the subscripts 1 and 2 stand for the injection and suction respectively, and θ_1 and θ_2 are the angles between the injection and suction slot's surface and a line normal to the airfoil chord[3]. α is the angle of attack.

The total lift and drag on the airfoil can then be expressed as:

$$D = R'_x - F_{x_{cfj}} \tag{5}$$

$$L = R'_y - F_{y_{cfj}} \tag{6}$$

where R'_x and R'_y are the surface integral of pressure and shear stress in x (drag) and y (lift) direction excluding the internal ducts of injection and suction. For CFJ wing simulations, the total lift and drag are calculated by integrating Eqs.(5) and (6) in the spanwise direction.

2.2 Jet Momentum Coefficient

The jet momentum coefficient C_μ is a parameter used to quantify the jet intensity. It is defined as:

$$C_\mu = \frac{\dot{m} V_j}{\frac{1}{2}\rho_\infty {V_\infty}^2 S} \tag{7}$$

where $\dot{m}$ is the injection mass flow, V_j is the mass-averaged injection velocity, ρ_∞ and V_∞ denote the free stream density and velocity, and S is the planform area.

2.3 Micro-compressor Power Coefficient

CFJ is implemented by mounting a pumping system inside the wing that withdraws air from the suction slot and blows it into the injection slot. The power consumption is determined by the jet mass flow and total enthalpy change as the following:

$$P = \dot{m}(H_{t1} - H_{t2}) \tag{8}$$

where H_{t1} and H_{t2} are the mass-averaged total enthalpy in the injection cavity and suction cavity respectively, P is the Power required by the pump and $\dot{m}$ the jet mass flow rate. Introducing P_{t1} and P_{t2} as the mass-averaged total pressure in the injection and suction cavity respectively, the compressor efficiency η, and the total pressure ratio of the pump $\Gamma = \frac{P_{t1}}{P_{t2}}$, the power consumption is expressed as:

$$P = \frac{\dot{m} C_p T_{t2}}{\eta}(\Gamma^{\frac{\gamma-1}{\gamma}} - 1) \tag{9}$$

where γ is the specific heat ratio equal to 1.3 for Martian air , C_p is the specific heat at constant pressure, T_t is the total pressure at the suction slot, η is the CFJ micro-compressor actuator efficiency. The power coefficient is expressed as:

$$P_c = \frac{P}{\frac{1}{2}\rho_\infty V_\infty^3 S} \tag{10}$$

2.4 Aerodynamic Efficiency

The conventional wing aerodynamic efficiency is defined as:

$$\frac{C_L}{C_D} \tag{11}$$

For the CFJ wing, the ratio above still represents the pure aerodynamic relationship between lift coefficient and drag coefficient. However since CFJ active flow control consumes energy, the ratio above is modified to take into account the energy consumption of the micro-compressor. The formulation of the corrected aerodynamic efficiency for CFJ wings is given in Eqn.1. If the micro-compressor power coefficient is set to 0, Eqn.1 returns to the aerodynamic efficiency of a conventional airfoil.

2.5 CFD Simulation Setup

The in house FASIP(Flow-Acoustics-Structure Interaction Package) CFD code is used to conduct the numerical simulation. The 3D Reynolds Averaged Navier-Stokes (RANS) equations with one-equation Spalart-Allmaras(SA) turbulence model is used. A 3rd order WENO scheme for the inviscid flux [28, 29, 30, 31, 32, 33] and a 2nd order central differencing for the viscous terms [28, 32] are employed to discretize the Navier-Stokes equations. The low diffusion E-CUSP scheme used as the approximate Riemann solver suggested by Zha et al [29] is utilized with the WENO scheme to evaluate the inviscid fluxes. Implicit time marching method using Gauss-Seidel line relaxation is used to achieve a fast convergence rate [34]. Parallel computing is implemented to save wall clock simulation time [35].

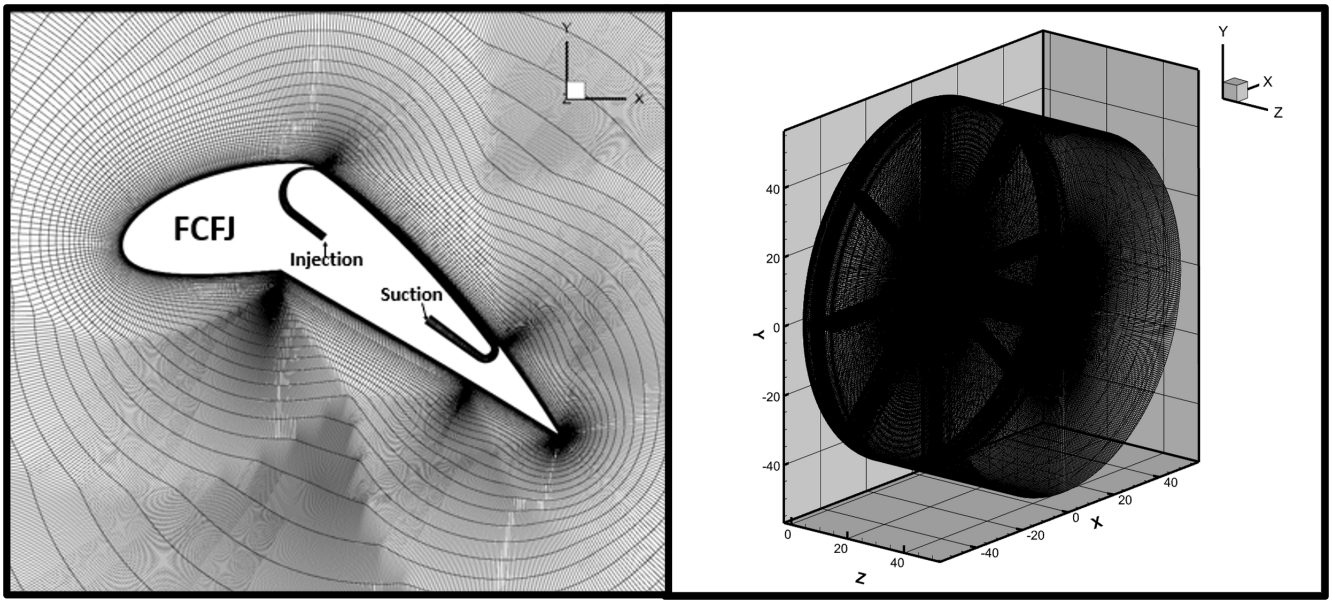

Figure 3: Computational mesh used in the current work.

2.6 Boundary Conditions

The 3rd order accuracy no slip condition is enforced on the solid surface with the wall treatment suggested in [36] to achieve the flux conservation on the wall. The far field boundary is located at 50 chord with a O-mesh topology. The computational mesh is shown in Fig. 3. Total pressure, total temperature and flow angles are specified at the upstream portion of the far field. Constant static pressure is applied at the downstream portion of the far field. The first grid point on the wing surface is placed at $y^+ \approx 1$.

The atmospheric properties for Mars, relevant to the present analysis, are summarized in Table 1.

Table 1: Flow Conditions and Properties

Variable	**Value**	**Unit**
p	655	[Pa]
T	220	[K]
ρ	0.01575	[kg/m^3]
μ	1.11E-05	[kg/m s]
R	188.9	[J/kg K]
L_{ref}	1	[m]
U_∞	39.53	[m/s]
γ	1.3	
M_∞	0.17	
Re_∞	5.63E+04	

3 Results and Discussion

3.1 2D Simulation

Preliminary 2D analyses were conducted under the conditions specified in Table 1 with Mach number of 0.17 and Reynolds number of 5.63×10^3. Table 2 presents the results for the NACA 6421 Baseline, demonstrating a maximum C_L of 0.98 with flow and revealing separation at very low angles of attack (AoA) of 0deg, as illustrated in Figure 4 - Figure 6. As noted in Mueller's study[**?**], thicker airfoils are more susceptible to separation in the low Reynolds number regime. However, as AoA increases to 10deg, the separation inception point migrates towards the leading edge, producing a massive flow separation. With the existence of flow separation at low AoA, the thick airfoil such as NACA 6421 is thous not suitable to be used for low Reynolds aircraft. Unlike at higher Reynolds numbers, the shear layer in this low Re regime lacks sufficient energy to transition into a turbulent boundary layer and reattach to the airfoil surface. This susceptibility to separation at the low Reynolds numbers stems from the combined effects of a stable laminar boundary layer, insufficient momentum in the shear layer, and the dominance of viscous forces, all of which hinder the transition to turbulence and reattachment necessary for efficient lift generation. Consequently, thick airfoils are generally avoided in the low Reynolds number regime, favoring very thin airfoils[37, 38, 39], which makes it more difficult to achieve a high lift coefficient.

Table 2: NACA 6421 Baseline Results

AoA	C_L	C_D	C_L/C_D	C_L^2/C_D
0	0.365	0.030	12.03	4.39
5	0.754	0.042	17.93	13.52
10	0.964	0.078	12.28	11.84
15	0.982	0.155	6.33	6.22
20	0.868	0.296	2.93	2.54

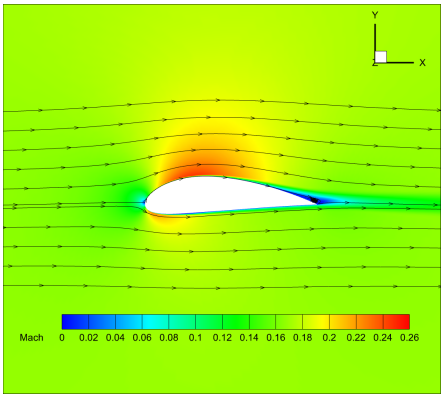

Figure 4: Baseline AoA 0°

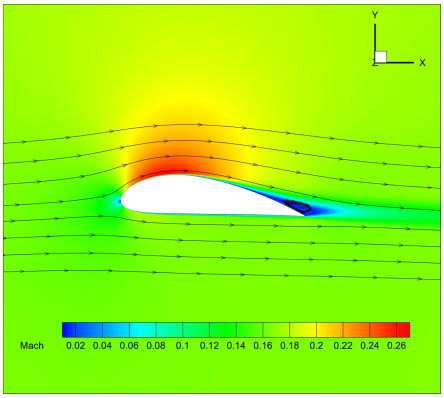

Figure 5: Baseline AoA 5°

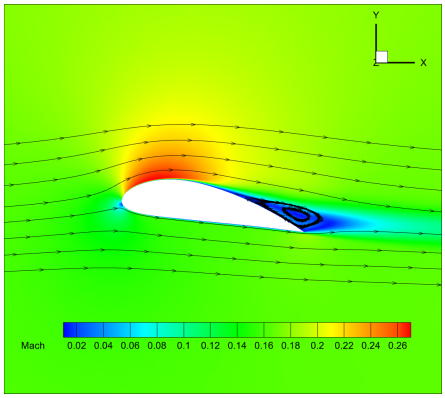

Figure 6: Baseline AoA 10°

Notably, we observe that FCFJ wing can achieve very high lift coefficients at cruise conditions, even in the low Reynolds number regime. The injection jet triggers the main flow boundary layer to become turbulent. It also energize the turbulent boundary layer to resist high adverse pressure gradient and keeps the flow attached. Table 3 presents the 2D FCFJ results for β of 10, 20, 30, and 35 degrees, and injection sizes of 0.4 %Cand 0.6 %C at the same Mach number of 0.17 and the Reynolds number of 5.63×10^3. While at low β angles the flow attaches well even with a small C_μ, at high β angles, a C_μ near 0.1 is required. At a deflection angle β of 10°, C_L more than doubles to 1.69 while maintaining similar aerodynamic efficiency. Notably, at β values of 30° and 35°, exceptionally high C_L values exceeding 3.5 are achieved without encountering separation. Remarkably, at $\beta = 30°$ and an injection size of 0.6 %C, we achieved a reasonable $(C_L/C_D)_c$ of 16.2 and a productivity efficiency of $(C_L^2/C_D)_c$ 56, an increase of more than four times over the baseline configuration. The corresponding flow fields are illustrated in Figures 7 and 8.

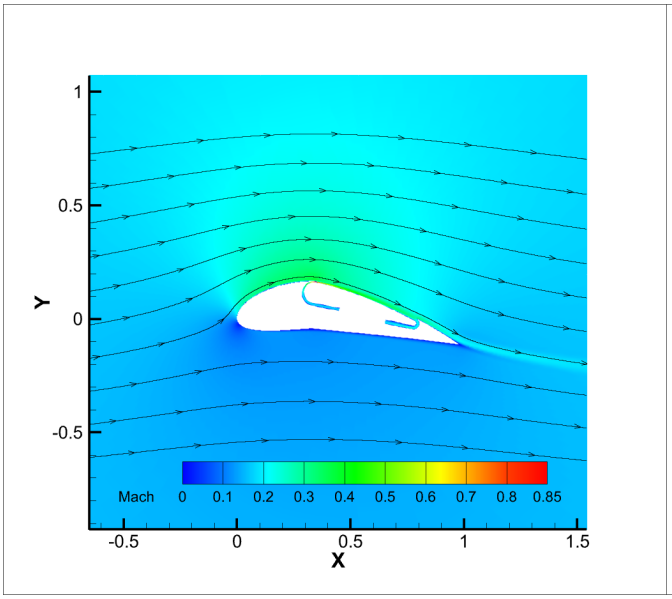

Figure 7: β 10° with C_μ=0.03

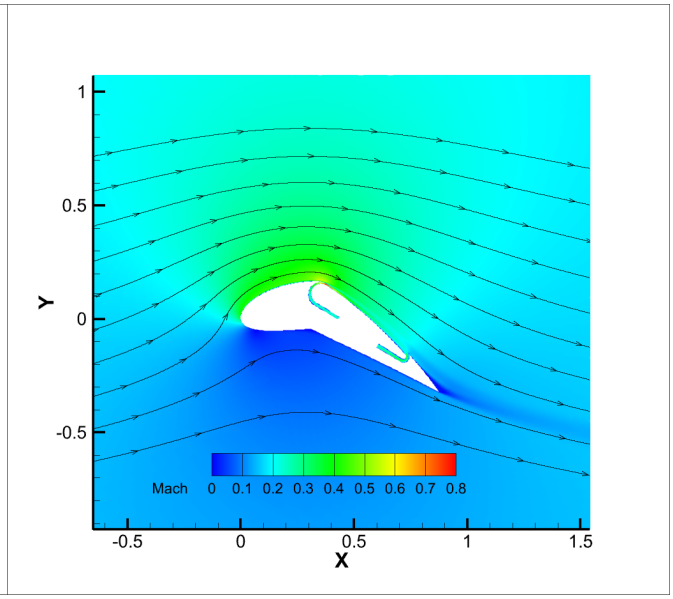

Figure 8: β 30° with C_μ=0.12

Table 3: 2D FCFJ Results

β	AoA	Inj %C	C_μ	C_L	C_D	C_L/C_D	Pt ratio	P_c	$(C_L/C_D)_c$	$(C_L^2/C_D)_c$
10	6.4	0.4	0.03	1.49	0.026	56.48	1.116	0.040	22.41	33.48
10	6.4	0.4	0.05	1.69	0.012	139.99	1.183	0.081	18.05	30.47
10	6.4	0.4	0.07	1.88	0.002	983.87	1.252	0.131	14.17	26.58
20	13.25	0.4	0.03	1.37	0.127	10.78	1.118	0.041	8.14	11.16
20	13.25	0.4	0.05	1.94	0.070	27.86	1.184	0.081	12.88	24.99
20	13.25	0.4	0.07	2.56	0.028	91.10	1.206	0.105	19.21	49.19
20	13.25	0.4	0.09	2.76	0.015	184.73	1.258	0.146	17.14	47.30
20	13.25	0.4	0.11	2.95	0.002	1330.60	1.317	0.196	14.88	43.94
30	20	0.4	0.07	2.90	0.058	49.78	1.319	0.161	13.26	38.47
30	20	0.4	0.08	3.32	0.036	92.73	1.326	0.174	15.85	52.62
30	20	0.4	0.09	3.49	0.027	127.7	1.349	0.194	15.75	54.97
30	20	0.4	0.1	3.61	0.021	171.2	1.378	0.219	15.05	54.32
30	20	0.4	0.12	3.85	0.012	327.0	1.448	0.279	13.24	50.94
30	20	0.6	0.1	3.19	0.044	72.7	1.292	0.161	15.59	49.75
30	20	0.6	0.12	3.51	0.029	122.28	1.317	0.188	16.20	56.86
30	20	0.6	0.15	3.80	0.015	256.7	1.366	0.240	14.92	56.74
35	23.5	0.4	0.08	3.06	0.081	37.69	1.340	0.186	11.43	34.98
35	23.5	0.4	0.1	3.72	0.048	77.96	1.367	0.220	13.89	51.66
35	23.5	0.4	0.12	4.03	0.036	111.8	1.424	0.271	13.12	52.92
35	23.5	0.6	0.1	3.18	0.077	41.18	1.277	0.199	11.53	36.67
35	23.5	0.6	0.12	3.60	0.055	65.41	1.291	0.224	12.88	46.31
35	23.5	0.6	0.15	4.04	0.038	105.245	1.340	0.283	12.54	50.62

3.2 3D Simulation

The 3D simulation is conducted at an Aspect Ratio (AR) of 20, maintaining the same conditions of Mach number 0.17 and Reynolds number 5.63×10^4 as used in the 2D trade study. Notably, AR 20 has demonstrated excellent performance at a higher Reynolds number of 3.48×10^6 and Mach number 0.17 [24]. Therefore, this aspect ratio is initially applied to the Martian conditions. Table 4 presents the results of the 3D wing with varying flap deflection angles and momentum coefficient. As depicted in Figure 9, C_L increases while C_L/C_D decreases as β increases. This is attributed to the rise in C_D as β with AoA increases. In Figure 10, it is observed that the corrected aerodynamic efficiency C_L/C_{D_c} decreases with increasing β, while the productivity efficiency C_L^2/C_{D_c} tends to increase. This occurs because both C_L/C_{D_c} and C_D rise as β increases, leading to higher power consumption for flow attachment at larger β values. However, since the productivity coefficient is proportional to the square of the lift coefficient, FCFJs capable of achieving very high lift coefficients can reach over C_L^2/C_{D_c} of 26 with a C_L of exceeding 3.5 at $\beta = 35°$.

Figure 11 illustrates the pressure ratio for injection sizes of 0.4%C and 0.6%C at β values of 30° and 35°. Notably, a lower pressure ratio is observed at 0.6%C with a larger injection size at the same β and similar C_L value. The case with $\beta = 35°$ and an injection size of 0.6%C at C_μ=0.15 achieves a pressure ratio of 1.3 at a C_L of 3.73, a C_L/C_{D_c} of 7, and a productivity efficiency C_L^2/C_{D_c} of 26.3, which is desirable. These findings underscore the significance of the compressor pressure ratio in practical FCFJ wing applications, highlighting the substantial influence of injection size on this critical parameter.

Table 4: 3D FCFJ Results for AR20

β	AoA	Cap	Inj %C	C_μ	C_L	C_D	C_L/C_D	Pt ratio	P_c	$(C_L/C_D)_c$	$(C_L^2/C_D)_c$
10	6.4	2C	0.4	0.03	1.40	0.098	14.2	1.116	0.041	10.01	13.99
10	6.4	2C	0.4	0.05	1.56	0.089	17.5	1.181	0.082	9.13	14.22
20	13.25	2C	0.4	0.07	2.38	0.141	16.9	1.212	0.109	9.54	22.75
30	20	2C	0.4	0.09	3.17	0.205	15.4	1.341	0.188	8.07	25.60
30	20	2C	0.4	0.1	3.30	0.211	15.6	1.377	0.217	7.71	25.49
30	20	2C	0.6	0.12	3.28	0.210	15.6	1.281	0.206	7.88	25.81
30	20	2C	0.6	0.13	3.38	0.215	15.7	1.303	0.230	7.61	25.72
30	20	2C	0.6	0.15	3.54	0.223	15.9	1.345	0.275	7.11	25.13
35	23.5	2C	0.4	0.09	3.45	0.259	13.3	1.351	0.200	7.50	25.85
35	23.5	2C	0.4	0.1	3.58	0.263	13.6	1.388	0.230	7.25	25.92
35	23.5	none	0.4	0.1	3.51	0.287	12.2	1.385	0.229	6.80	23.84
35	23.5	2C	0.4	0.12	3.82	0.278	13.7	1.471	0.299	6.62	25.26
35	23.5	2C	0.6	0.12	3.43	0.260	13.2	1.250	0.193	7.56	25.91
35	23.5	2C	0.6	0.13	3.53	0.263	13.4	1.266	0.212	7.44	26.27
35	23.5	2C	0.6	0.15	3.73	0.272	13.7	1.303	0.255	7.07	26.34

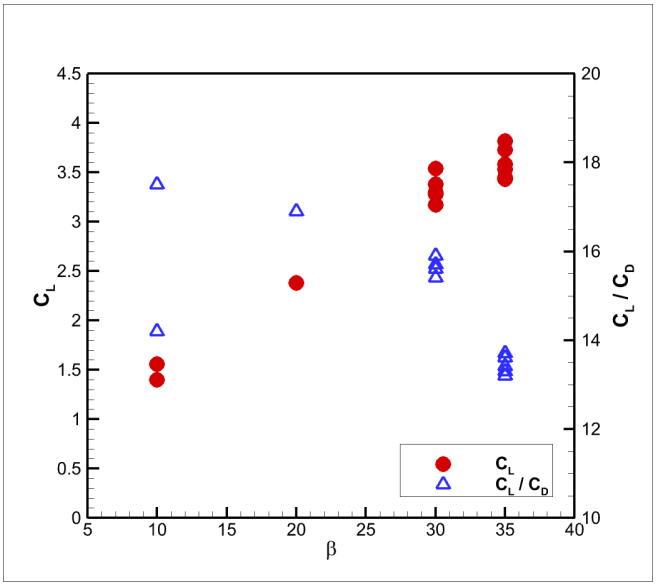

Figure 9: C_L and C_L/C_D according to β

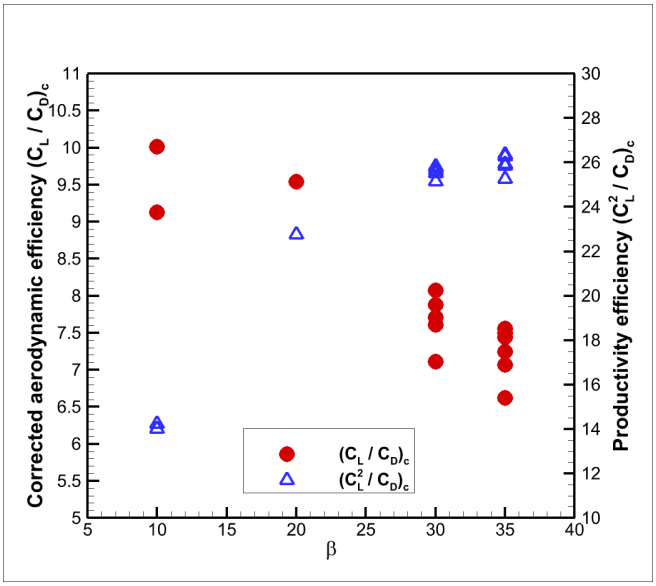

Figure 10: $(C_L/C_D)_c$ and $(C_L^2/C_D)_c$ according to β

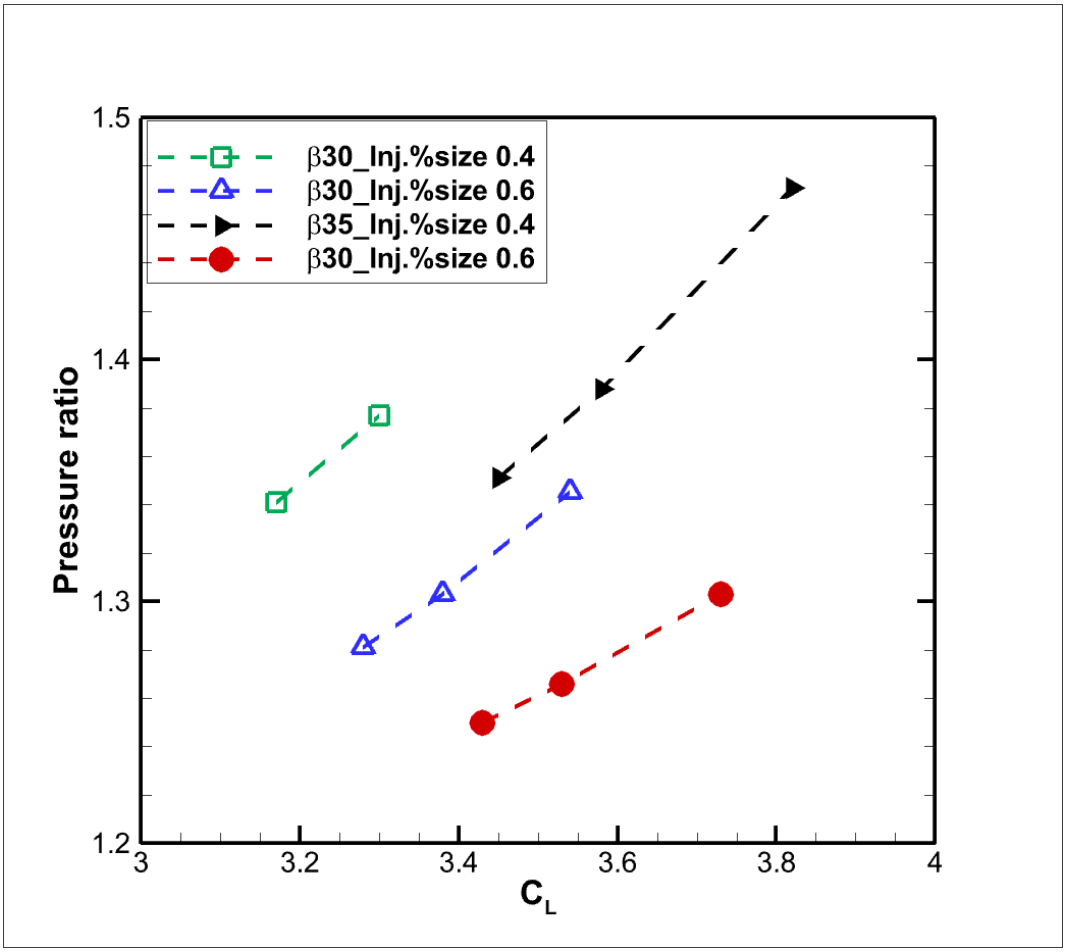

Figure 11: Injection size effect for pressure ratio

Figure 12 shows the flow field and surface pressure coefficient of the 3D wing simulation without a tip cap. At Root and 50% span, it can be seen that C_p continues from the leading edge to the injection with a very high peak near the injection. A strong vortex occurs near the tip as shown in Figure 11, and the C_p value is also low overall. In Table 4, C_L for this case is 3.51, and $(C_L/C_D)_c$ is 6.8, which is reduced by 6% and 51%, respectively, compared to 2D due to the 3D tip vortex effect.

Figure 13 illustrates the flow field C_p distribution when a circular tip cap with a diameter twice the airfoil chord is installed at the tip to mitigate the tip vortex effect. The flow characteristics at the root and 50% span remain largely similar to the configuration without the tip cap. The cap effectively mitigates the tip vortex, leading to a reduction in C_D and a subsequent increase in $(C_L/C_D)_c$ of approximately 6.6%, as detailed in Table 4. Building upon this beneficial effect, the same cap configuration is applied to other cases, yielding further performance improvements.

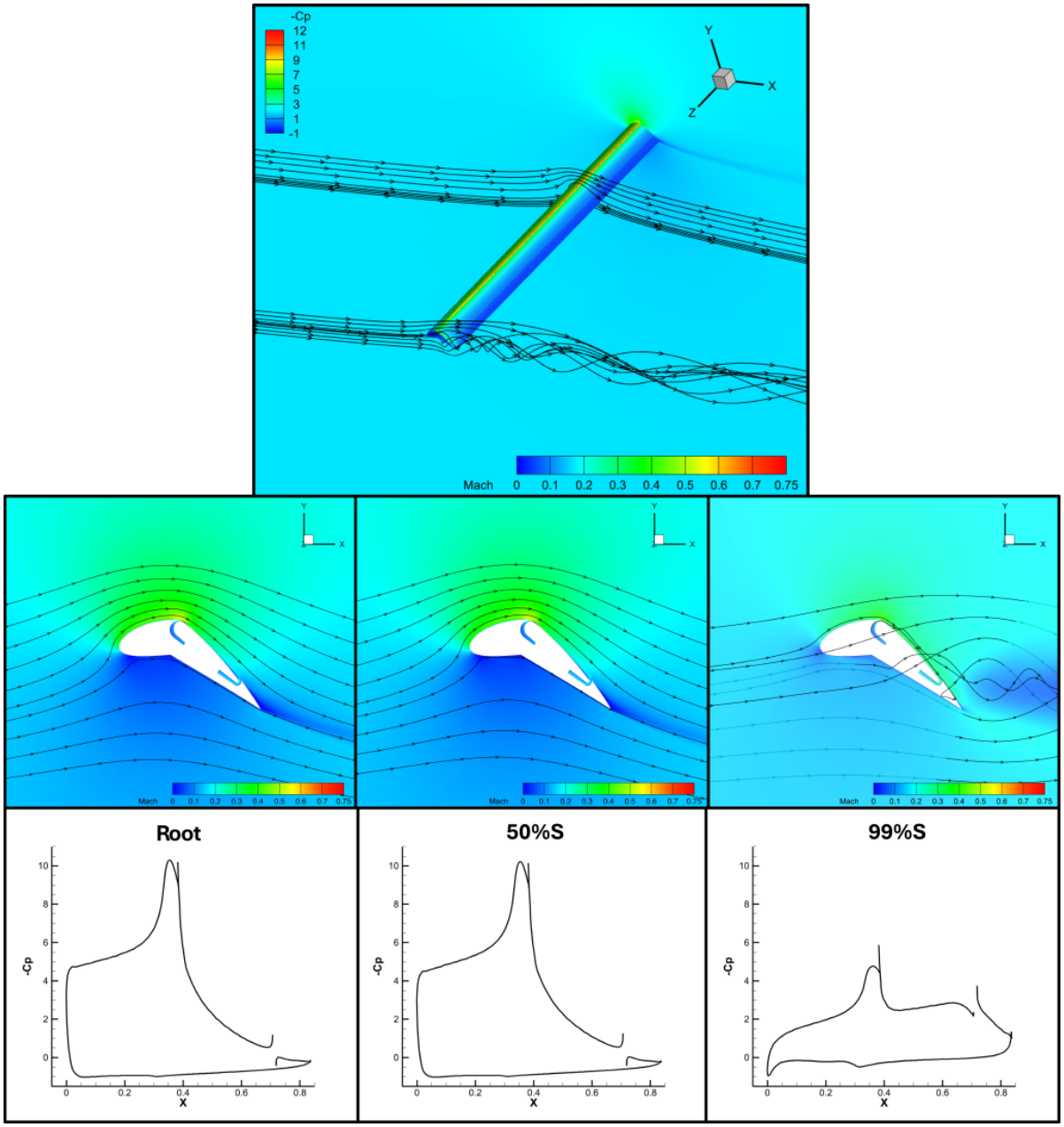

Figure 12: FCFJ flow field and pressure coefficient without cap(β=35°, injection size=0.4%C, C_μ=0.1)

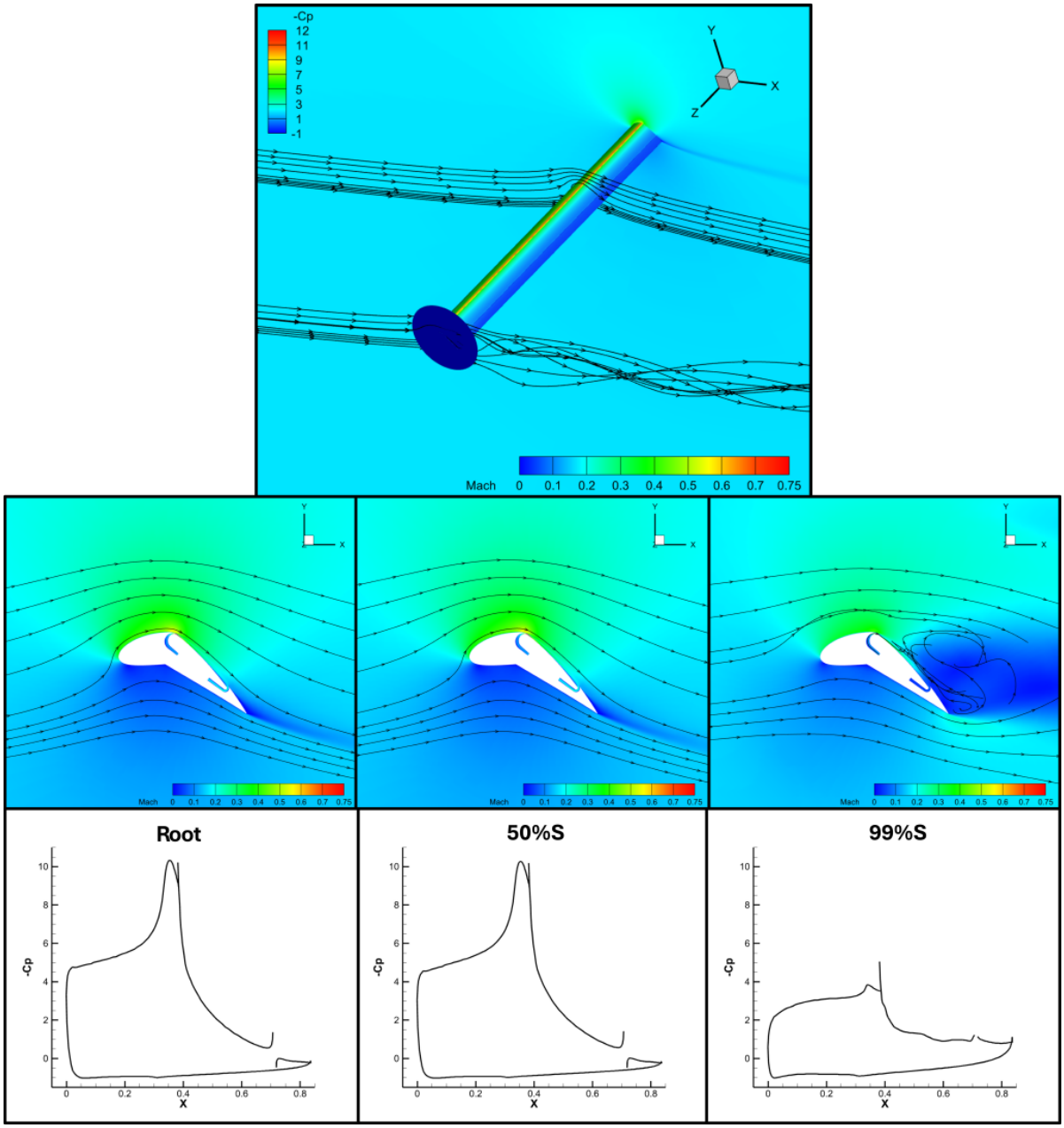

Figure 13: FCFJ flow field and pressure coefficient with cap(β=35°, injection size=0.4%C, C_μ=0.1)

4 Conclusion

This paper presents a numerical investigation of 2D and 3D Flapped Coflow Jet (FCJF) airfoils and wing designed for low Reynolds number operation in Martian conditions. The simulation is conducted at a Mach number (Ma) of 0.17 and a Reynolds number (Re) of 5.63E+04, aligning with realistic flight operating conditions. The FCFJ airfoil is derived from the NACA 6421 baseline geometry. Preliminary analysis confirms the NACA 6421 baseline's unsuitability for Mars due to its susceptibility to separation at low Reynolds numbers even at low AoA of 0deg.

In contrast, the FCFJ airfoil exhibits high performance, maintaining attached flow even at a high flap deflection angle β of 35° and achieving a very high cruise lift coefficient C_L exceeding 3.5, coupled with a corrected lift-to-drag ratio $(C_L/C_D)_c$ of 16 in 2D simulation. Extending this investigation to 3D, the effects of tip vortices become evident, resulting in a $(C_L/C_D)_c$ less than half of its 2D counterpart. To mitigate these adverse effects, a tip cap is introduced, demonstrating a 6.6% improvement in $(C_L/C_D)_c$ under identical conditions. Notably, a larger injection size significantly decreases the compressor pressure ratio, with as increase of 7-9% by decreasing the injection size from 0.6%C to 0.4%C at a comparable C_L and β of 35°.

Overall the FCFJ wing demonstrates the ability to achieve remarkably high cruise lift coefficients exceeding 3.5, with a productivity efficiency of 26 and a reasonable $(C_L/C_D)_c$ of 7.5. This breakthrough has laid an important foundation to fly fixed wing aircraft in Martian atmosphere by dramatically reducing aircraft size and weight, and increased payloads.

5 Acknowledgment

The authors would like to acknowledge the computing resources provided by the Center of Computational Sciences (CCS) at the University of Miami. The teaching assistantship support from the University of Miami is also acknowledged.

Disclosure: The University of Miami and Dr. Gecheng Zha may receive royalties for future commercialization of the intellectual property used in this study. The University of Miami is also equity owner in CoFlow Jet, LLC, licensee of the intellectual property used in this study.

References

[1] Koji FUJITA, Remi LUONG, Hiroki NAGAI, Keisuke ASAI, "Conceptual Design of Mars Airplane," *Trans. JSASS Aerospace Tech. Japan, Vol.10, No.ists28, pp.5-10*, 2012.

[2] G.-C. Zha and D. C. Paxton, "A Novel Flow Control Method for Airfoil Performance Enhancement Using Co-Flow Jet." *Applications of Circulation Control Technologies*, Chapter 10, p. 293-314, Vol. 214, Progress in Astronautics and Aeronautics, AIAA Book Series, Editors: Joslin, R. D. and Jones, G.S., 2006.

[3] G.-C. Zha, W. Gao, and C. Paxton, "Jet Effects on Co-Flow Jet Airfoil Performance," *AIAA Journal, No. 6,*, vol. 45, pp. 1222–1231, 2007.

[4] G.-C. Zha, C. Paxton, A. Conley, A. Wells, and B. Carroll, "Effect of Injection Slot Size on High Performance Co-Flow Jet Airfoil," *AIAA Journal of Aircraft*, vol. 43, 2006.

[5] G.-C. Zha, B. Carroll, C. Paxton, A. Conley, and A. Wells, "High Performance Airfoil with Co-Flow Jet Flow Control," *AIAA Journal*, vol. 45, 2007.

[6] Wang, B.-Y. and Haddoukessouni, B. and Levy, J. and Zha, G.-C., "Numerical Investigations of Injection Slot Size Effect on the Performance of Co-Flow Jet Airfoil," *Journal of Aircraft*, vol. Vol. 45, No. 6,, pp. pp.2084–2091, 2008.

[7] B. P. E. Dano, D. Kirk, and G.-C. Zha, "Experimental Investigation of Jet Mixing Mechanism of Co- Flow Jet Airfoil." AIAA-2010-4421, 5th AIAA Flow Control Conference, Chicago, IL, 28 Jun - 1 Jul 2010.

[8] B. P. E. Dano, G.-C. Zha, and M. Castillo, "Experimental Study of Co-Flow Jet Airfoil Performance Enhancement Using Micro Discreet Jets." AIAA Paper 2011-0941, 49th AIAA Aerospace Sciences Meeting, Orlando, FL, 4-7 January 2011.

[9] A. Lefebvre, B. Dano, W. Bartow, M. Fronzo, and G. Zha, "Performance and energy expenditure of coflow jet airfoil with variation of mach number," *Journal of Aircraft*, vol. 53, no. 6, pp. 1757–1767, 2016.

[10] A. Lefebvre, G-C. Zha, "Numerical Simulation of Pitching Airfoil Performance Enhancement Using Co-Flow Jet Flow Control," *AIAA paper 2013-2517*, June 2013.

[11] A. Lefebvre, G-C. Zha, "Cow-Flow Jet Airfoil Trade Study Part I : Energy Consumption and Aerodynamic Performance," *Proceedings of the AIAA Flow Control Conference*, June 2014.

[12] A. Lefebvre, G-C. Zha, "Cow-Flow Jet Airfoil Trade Study Part II : Moment and Drag," *Proceedings of the AIAA Flow Control Conference*, June 2014.

[13] Yunchao Yang, Gecheng Zha, "Super-Lift Coefficient of Active Flow Control Airfoil: What is the Limit?," *AIAA Paper 2017-1693, AIAA SCITECH2017, 55th AIAA Aerospace Science Meeting, Grapevine, Texas, 9-13 January 2017*, 2017.

[14] Gecheng Zha, Yunchao Yang, Yan Ren, Brendan McBreen, "Super-Lift and Thrusting Airfoil of Coflow Jet Actuated by Micro-Compressors," *AIAA Paper-2018-3061, AIAA AVIATION Forum 2018, Flow Control Conference, June 25-29*, 2018.

[15] Lefebvre, A. and Zha, G.-C., "Trade Study of 3D Co-Flow Jet Wing for Cruise Performance." AIAA Paper 2016-0570, AIAA SCITECH2016, AIAA Aerospace Science Meeting, San Diego, CA, 4-8 January 2016.

[16] Kewei Xu, Gecheng Zha, "High Control Authority 3D Aircraft Control Surfaces Using Co-Flow Jet," *AIAA Journal of Aircraft*, 2020.

[17] Kewei Xu, Yan Ren, Gecheng Zha, "Numerical Analysis of Energy Expenditure for Co-Flow Wall Jet Separation Control," *AIAA Journal, published online: 11 Jan 2022, doi.org/10.2514/1.J061015*, 2022.

[18] B. McBreen, K.-W. Xu, G.-C. Zha, "Numerical Study of Extreme Adverse Pressure Gradients Enabled by Co-Flow Jet," *AIAA Paper-2023-1430, AIAA SCITECH 2023 Forum, 23-27 January 2023, National Harbor, MD*, 2023.

[19] B. McBreen, Y.-C. Yang, G.-C. Zha, "Improved Delayed Detached Eddy Simulation of Co-Flow Jet Flow Control in Extreme Adverse Pressure Gradients," *AIAA paper 2024-0063, AIAA SCITECH 2024 Forum, 8-12 January 2024, Orlando, FL*, 2024.

[20] Yang Wang and Gecheng Zha, "Study of Mach Number Effect for 2D Co-Flow Jet Airfoil at Cruise Conditions," *AIAA Paper 2019-3169, AIAA Aviation 2019 Forum, 17-21 June 2019, Dallas, Texas*, 2019.

[21] Yan Ren, Gecheng Zha, "Performance Enhancement by Tandem Wings Interaction of CoFlow Jet Aircraft," *AIAA Paper 2021-1823, AIAA SciTech Forum, 11–15; 19–21 January 2021, VIRTUAL EVENT*, 2021.

[22] Yang Wang, Yunchao Yang and Gecheng Zha, "Study of Super-Lift Coefficient of Co-Flow Jet Airfoil and Its Power Consumption," *AIAA Paper 2019-3652, AIAA Aviation 2019 Forum, 17-21 June 2019, Dallas, Texas* , 2019.

[23] Jaehyoung Jeon, Yan Ren, and Gecheng Zha, "Toward Ultra-High Cruise Lift Coefficient Using Flapped CoFlow Jet Airfoil," *AIAA SciTech Forum, January 23-27*, 2023.

[24] Jaehyoung Jeon, Brendan McBreen, Yan Ren, and Gecheng Zha, "Study of 3D Flapped CoFlow Jet Wings for Ultra-High Cruise Lift Coefficient," *AIAA Aviation Forum, June 12-16*, 2023.

[25] Jaehyoung Jeon, Yan Ren, and Gecheng Zha, "Flapped CoFlow Jet Airfoil for High Lift Cruise at Low Reynolds Number in Martian Atmosphere," *AIAA SciTech Forum, January 8-12*, 2024.

[26] Zha, G.-C,, "Feasibility Study of Deflected Slipstream Airfoil for VTOL Hover Enabled by CoFlow Jet," *Proceedings of AIAA Aviation Forum 2023, 12–16 June 2023, San Diego, CA*, 2023.

[27] Kewei Xu, Gecheng Zha, "Enhancing aircraft control surface effectiveness by co-flow jet flap at low energy expenditure," *Elsevier Journal of Aerospace Science and Technology 133 (2023) 108145, https://doi.org/10.1016/j.ast.2023.108145*, 2023.

[28] Y.-Q. Shen and G.-C. Zha, "Large Eddy Simulation Using a New Set of Sixth Order Schemes for Compressible Viscous Terms ," *Journal of Computational Physics*, vol. 229, pp. 8296–8312, 2010.

[29] Zha, G.C., Shen, Y.Q. and Wang, B.Y., "An improved low diffusion E-CUSP upwind scheme ," *Journal of Computer and Fluids*, vol. 48, pp. 214–220, Sep. 2011.

[30] Y.-Q. Shen and G.-Z. Zha , "Generalized finite compact difference scheme for shock/complex flowfield interaction," *Journal of Computational Physics*, vol. doi:10.1016/j.jcp.2011.01.039, 2011.

[31] Shen, Y.-Q. and Zha, G.-C. and Wang, B.-Y., " Improvement of Stability and Accuracy of Implicit WENO Scheme," *AIAA Journal*, vol. 47, No. 2, pp. 331–344, 2009.

[32] Shen, Y.-Q. and Zha, G.-C. and Chen, X.-Y., " High Order Conservative Differencing for Viscous Terms and the Application to Vortex-Induced Vibration Flows," *Journal of Computational Physics*, vol. 228(2), pp. 8283–8300, 2009.

[33] Shen, Y.-Q. and Zha, G.-C. , " Improvement of the WENO Scheme Smoothness Estimator," *International Journal for Numerical Methods in Fluids*, vol. DOI:10.1002/fld.2186, 2009.

[34] G.-C. Zha and E. Bilgen, "Numerical Study of Three-Dimensional Transonic Flows Using Unfactored Upwind-Relaxation Sweeping Algorithm," *Journal of Computational Physics*, vol. 125, pp. 425–433, 1996.

[35] B.-Y. Wang and G.-C. Zha, "A General Sub-Domain Boundary Mapping Procedure For Structured Grid CFD Parallel Computation," *AIAA Journal of Aerospace Computing, Information, and Communication*, vol. 5, No.11, pp. 2084–2091, 2008.

[36] Y.-Q. Shen, G.-C. Zha, and B.-Y. Wang, "Improvement of Stability and Accuracy of Implicit WENO Scheme ," *AIAA Journal*, vol. 47, pp. 331–344, 2009.

[37] Witold J.F.Koning, Wayne Johnson, Allan, "Generation of Mars Helicopter Rotor Model for Comprehensive Analyses," *Aeromechanics Design for Transformative Vertical Flight, San Francisco, California, USA, January 16-18, 2018*, 2018.

[38] Witold J.F.Koning, Ethan A.Romander, Wayne Johnson, "Optimization of Low Reynolds Number Airfoils for Martian Rotor Applications Using an Evolutionary Algorithm," *AIAA SciTech, Orlando, Florida, USA*, 2020.

[39] Justin Winslow, Hikaru Otsuka, Bharath Govindarajan, Inderjit Chopra, "Basic Understanding of Airfoil Characteristics at Low Reynolds Numbers (1E4 – 1E5)," *JOURNAL OF AIRCRAFT, Vol. 55, No. 3*, 2018.